Structural Engineering and Mechanics, *Vol. 75, No. 6 (2020) 643-657*
DOI: https://doi.org/10.12989/sem.2020.75.6.643

Test and simulation of circular steel tube confined concrete (STCC) columns made of plain UHPC

Phong T. Le[1], An H. Le*[2] and Lai Binglin[3]

[1]Thuyloi University, 175 Tay son, Dong da, Hanoi, Vietnam
[2]NTT Hi-Tech Institute, Nguyen Tat Thanh University, Ho Chi Minh City, Vietnam
[3]Department of Civil and Environmental Engineering, National University of Singapore

(Received October 2, 2019, Revised June 23, 2020, Accepted July 21, 2020)

Abstract. This study presents experimental and numerical investigations on circular steel tube confined ultra high performance concrete (UHPC) columns under axial compression. The plain UHPC without fibers was designed to achieve a compressive strength ranged between 150 MPa and 200 MPa. Test results revealed that loading on only the UHPC core can generate a significant confinement effect for the UHPC core, thus leading to an increase in both strength and ductility of columns, and restricting the inherent brittleness of unconfined UHPC. All tested columns failed by shear plane failure of the UHPC core, this causes a softening stage in the axial load versus axial strain curves. In addition, an increase in the steel tube thickness or the confinement index was found to increase the strength and ductility enhancement and to reduce the magnitude of the loss of load capacity. Besides, steel tube with higher yield strength can improve the post-peak behavior. Based on the test results, the load contribution of the steel tube and the concrete core to the total load was examined. It was found that no significant confinement effect can be developed before the peak load, while the ductility of post-peak stage is mainly affected by the degree of the confinement effect. A finite element model (FEM) was also constructed in ABAQUS software to validate the test results. The effect of bond strength between the steel tube and the UHPC core was also investigated through the change of friction coefficient in FEM. Furthermore, the mechanism of circular steel tube confined UHPC columns was examined using the established FEM. Based on the results of FEM, the confining pressures along the height of each modeled column were shown. Furthermore, the interaction between the steel tube and the UHPC core was displayed through the slip length and shear stresses between two surfaces of two materials.

Keywords: UHPC; steel tube; axial compression; confinement effect; confinement index; FEM

1. Introduction

In recent times, there has been an accelerating interest in the utilization of ultra high performance concrete (UHPC) in construction throughout the world (An and Fehling 2017a, Graybeal 2005). This is mainly attributable to the superior mechanical properties offered by UHPC such as an extremely high compressive strength up to 200 MPa, a post-cracking tensile strength approaching 5MPa, and an excellent durability (An and Fehling 2017d, Graybeal 2005, Zohrevand and Mirmiran 2011). Furthermore, it has been found that UHPC is a potential material and a suitable alternative to normal strength concrete (NSC) or high strength concrete (HSC) as reduced size and increased load-bearing capacity of structural members can be achieved (Liew and Xiong 2012, Tue *et al.* 2004a, An and Fehling 2017a, Empelmann *et al.* 2008). A considerable effort has been put into investigating beneficial applications of UHPC and possibilities to develop novel structural elements with the employment of UHPC (Xiong *et al.* 2017, Empelmann *et al.* 2008, Tue *et al.* 2004b). However, the inherent brittleness of UHPC causes some obstacles for its utilization, especially for the columns or support structures in seismically active regions or in the members subjected to very high compressive loads (Liew and Xiong 2012, Xiong *et al.* 2017). In view of the fact that lateral confinement of concrete can lead to significant enhancements in both compressive strength and ductility, there have been several studies on the confining solutions to prevent the brittleness of UHPC columns (An and Fehling 2017a, Empelmann *et al.* 2004). These confining solutions for UHPC essentially include: (1) external confinement using fiber reinforced polymer (FRP) or steel tube (Zohrevand and Mirmiran 2011); (2) internal confinement using transverse reinforcement (Yang *et al.* 2015, Shin *et al.* 2015). Among such solutions, circular steel tube confined concrete (STCC) columns have emerged as an attractive option because of the efficient composite action of the concrete core and the steel tube to form a high performance member that benefits from significant increases in strength and ductility as compared to unconfined concrete members (An and Fehling 2017b, Giakoumelis and Lam 2004, De Oliveira *et al.* 2010, Han *et al.* 2005). Moreover, it is well known that STCC columns is a special type of concrete filled steel tube (CFST) columns where the load is applied to the concrete core only instead of applying to the entire section (Han *et al.* 2005, Yu *et al.* 2010, Ding *et al.* 2017). This loading pattern can generate a maximal confinement effect for the

*Corresponding author, Ph.D.
E-mail: lhan@ntt.edu.vn

http://www.techno-press.com/journals/sem&subpage=7
ISSN: 1225-4568 (Print), 1598-6217 (Online)

concrete core because in this situation, the steel tube mainly works to provide the lateral pressure to the concrete core (Ding *et al.* 2017; Liu *et al.* 2009, 2016; Johansson and Gylltoft 2002).

For the construction, the use of STCC columns makes the reinforced concrete (RC) beam to CFST column connection easier (Yu *et al.* 2010). When STCC columns are adopted for the connection, the outer steel tube does not pass the beam – column joint to ensure that the reinforcement in the composite columns and RC beam can pass through each other and work together. By means of STCC columns, the outer steel tube carries smaller direct axial loading through the bond and friction between the concrete core and steel tube as compared to CFST columns (Liu *et al.* 2009). Accordingly, the outer steel tube only serves to confine the RC columns. Therefore, the steel tube in STCC column shows a better confinement effect on the concrete core than that in CFST columns (An and Fehling 2017b). In practice, the steel reinforcements or steel sections usually embedded in the concrete core of STCC columns to resist the flexural moments and tensile forces for the connection (Liu *et al.* 2016).

It should be noted that the addition of fibers does not significantly increase the compressive strength of UHPC (An and Fehling 2017d). Moreover, previous study by Yan and Feng (2008) indicated that for the concrete filled steel tube column with the employment of UHPC, there is no notable effect on the strength and ductility when fibers was added even with the volume up to 2%. Therefore, fibers should not be used for this column type because the benefit for strength and ductility is minor, while the cost for construction signficantly increases. In the past, the majority of studies on STCC or CFST columns were mainly concerned with NSC or HSC. To date, research on the compressive behavior of STCC columns using UHPC has remained very limited with only a handful of studies reported (e.g., Tue *et al.* 2004a, b; Liew and Xiong 2012; Xiong *et al.* 2017; An and Fehling 2017a, b, c). Besides, all current design codes for composite columns have a limitation on the concrete strength, in which UHPC with the compressive strength higher than 150 MPa is certainly not covered and considered (Aslani *et al.* 2015; An and Fehling 2017a, b).

Based on the issues as highlighted above, this paper is aimed at providing experimental investigation on circular STCC columns using UHPC without the employment of fibers (CSTC-UHPC columns). The axially compressive behavior of six tested columns having the same outer diameter of 152.4 mm and three nominal steel thicknesses of 8.8, 6.3, and 5.0 mm is presented. The impact of some main parameters including steel tube thickness, column length on the strength and ductility is also explored. Subsequently, based on the test results, the load contribution of the steel tube and the UHPC core to the total load is examined. Finally, a comparison between finite element model (FEM) in ABAQUS software and test results is conducted. The effect of the friction coefficient between the UHPC core and the steel tube on load-shortening curve, confining curve, shear stress, and slip length is examined using the results of FEM.

2. Summary of experiment

2.1 Material properties

The mechanical properties of steel tube consisting of the yield strength (f_y), and elastic modulus (E_s) were determined by tensile coupons tests in accordance with EN 10002-1 (see Fig. 1a). UHPC mixtures without the use of steel fibers were produced based on the recipe of M3Q developed at University of Kassel (An and Fehling 2017d). The details of mix proportions for UHPC in this study are given in Table 1. The M3Q mixture possesses a very high self-compacting characteristic, thereby eliminating the necessity for compactness of concrete using external vibration. This is favorable for the casting UHPC on site and provides a great convenience during the preparation of test specimens. There were three batches of UHPC mixes corresponding to three steel thicknesses of test specimens (see Table 2). The flowability of the fresh concrete for each mix was checked immediately after mixing, using a mini-slump cone on a flow table in accordance with DIN EN 12350-8:2010-12 (see Fig. 1c). The average slump flow for fresh UHPC was found to be about 850 mm. The compressive strengths (f_c) and elastic modulus (E_c) were determined from three cylindrical specimens of 100 mm x 200 mm for each concrete batch in accordance with DIN EN 12390-3:2009-07 and DIN 1048-5, respectively (see Fig. 1b). The average values of f_y, E_s, f_c, E_c for each UHPC batch were given in Table 2.

2.2 Configuration of specimens

A total of six specimens, including three CSTC-UHPC stub columns and three CSTC-UHPC intermediate columns, were fabricated and tested under pure axial compression. The length of composite columns was classified in accordance with AIJ (2001) standard, in which the short column is defined as having a length-to-diameter ratio (L/D) smaller than 4 and the intermediate column refers to a ratio of L/D ranged between 4 and 12. All specimens had a same nominal outer diameter of steel tube (D) of 152.4 mm. Three nominal steel tube thicknesses (t) of 5.0, 6.3, and 8.8 mm were used for the tests. To facilitate the loading application to the concrete core only, the length of the concrete core (L_c) was designed to be 50 mm smaller than the length of the steel tube (L) (see Fig. 2). The dimensions of the test specimens are tabulated in Table 2 and described in Fig. 2.

Table 1 Composition of UHPC mix

Mix composition	Unit	UHPC
Water	kg/m^3	187.98
CEM I 52.5R HS-NA	kg/m^3	795.40
Silica fume	kg/m^3	168.60
Sika Viscorete 2810	kg/m^3	24.10
Ground Quartz W12	kg/m^3	198.40
Quartz sand 0.125/0.5	kg/m^3	971.00

a) Tension test on steel coupons b) Compression test on UHPC cylinder c) Slump flow of fresh UHPC mixture

Fig. 1 Reference tests to determine mechanical properties of steel tube (a) and UHPC (b, c)

Fig. 2 Schematic view and photos of specimens

Table 2 Material properties of specimens

Cast	Specimens	f_c (MPa)	E_c (GPa)	f_y (MPa)	E_s (GPa)
1	SF0-t8.8-L600 SF0-t8.8-L1000	178.9	48.37	392.6	197.7
2	SF0-t6.3-L600 SF0-t6.3-L1000	198.0	46.94	373.4	201.4
3	SF0-t5.0-L600 SF0-t5.0-L1000	190.4	46.19	445.9	197.9

Table 3 Dimensions of specimens

Specimens	L (mm)	L_c (mm)	D (mm)	t (mm)
SF0-t8.8-L600	600	551.9	152.4	8.8
SF0-t8.8-L1000	1000	942.9		
SF0-t6.3-L600	600	553.0	152.4	6.3
SF0-t6.3-L1000	1000	949.7		
SF0-t5.0-L600	600	552.3	152.4	5.0
SF0-t5.0-L1000	1000	948.5		

2.3 Fabrication of specimens

A formwork for filling UHPC into the steel tube was designed to ensure that the steel tube remained concentric during the process of concrete pouring, as shown in Fig. 3(a). Bottom stiff blocks were included in advance in the formworks. Due to very high slump flow, UHPC mixture was vertically poured into the steel tube without any additional vibrations, as shown in Fig. 3(b).

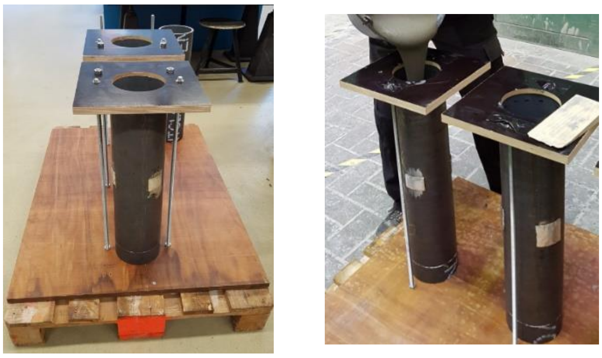

a) Formworks b) Pouring UHPC

Fig. 3 Fabrication of specimens

For installation of the upper stiff steel blocks and the symmetry of the columns, the concrete was filled up to a level which is roughly 25 mm lower than the top end of the steel tube as demonstrated in Fig. 2. Once the casting was complete, the top faces of the columns were covered and sealed using plastic sheet. Then all specimens were cured at ambient temperature in the laboratory. The height of the concrete core (L_c) and the steel tube (L) were carefully measured and given in Table 3.

2.4 Test setup and loading procedure

The load was applied on the concrete core only through two stiff steel blocks which had a height of 90 mm and a diameter smaller than that of UHPC core (see Fig. 4a and Fig. 4b). Prior to testing, the top surface of the concrete core was capped using a very thin layer of sand (about 4 mm) to

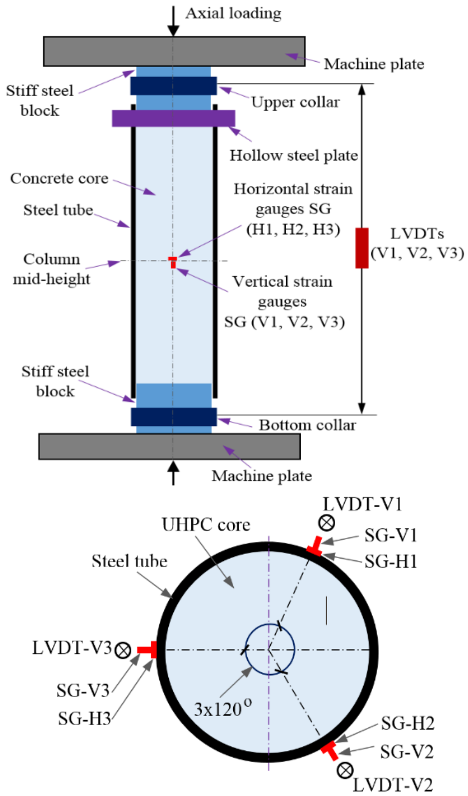

(a) Schematic view of test setup

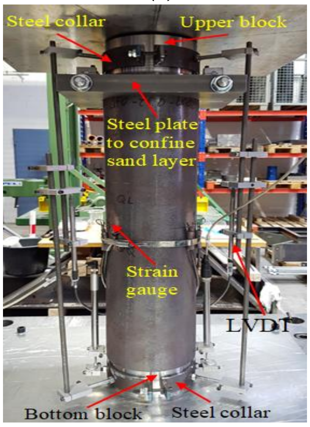

(a) Test setup

(b) Top capping using sand layer

Fig. 4 Test setup and top capping

create a flat surface and to ensure an even distribution of axial loading during testing (see Fig. 4c). Additionally, a steel plate with a circular hole was also produced and used to confine the column at the position of sand layer, thereby avoiding a premature local failure due to lateral pressure on the steel tube induced by the sand layer (see Fig. 4c).

To monitor the longitudinal and the hoop strain of the steel tube, six unidirectional strain gauges were attached to the external surface at the mid-height of the steel tube and placed at 120° spacing around the steel tube perimeter. Each column was instrumented with three strain gauges (SG-V1, SG-V2, SG-V3) installed in the longitudinal direction and three strain gauges (SG-H1, SG-H2, SG-H3) installed in the transverse direction. Axial shortening displacements of the specimen were recorded using three Linear Varying

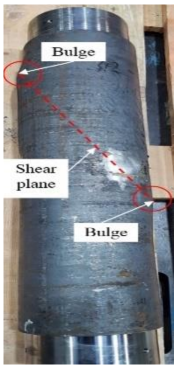

a) Short column

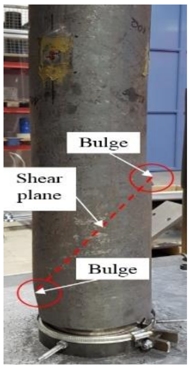

b) Intermediate column

c) Oblique slip

Fig. 5 Typical failure modes of test specimens

Displacement Transducers (LVDTs - V1, V2, V3), which were mounted on circular steel collars and placed along the specimen. These three LVDTs were also located at 120° apart and coincident with the position of the strain gauges. Fig. 4 show the test setup and instrumentations. All specimens were tested under uniaxial compression using a 6300 kN capacity computer-controlled universal compression testing machine. The loading rate for each specimen was set as 0.01 mm/s up to the ultimate load. This process was observed to be continued well beyond the ultimate load. When the performance of post-peak branch was fully captured at the axial displacements of LVDTs of about 15 mm, the displacement rate was changed to 0.05 mm/s. The testing was finished when the axial displacements of LVDTs reached a value of 20 mm. The duration of loading for each specimen ranged between 25 and 30 minutes.

3. Results and observations of experiment

3.1 Failure modes

In contradiction to the brittle behavior of unconfined UHPC cylinders in compression test there was no loud cracking/crushing noise emanating from the UHPC core around the ultimate load for all columns. All columns demonstrated a shear failure. When the load reached the ultimate load, oblique slip lines appeared on the outer walls of the steel tube and subsequently expanded along the height of the steel tube, as shown in Fig. 5(c). After testing, two outward bulges were observed at two opposite sides of the columns, as shown in Figs. 5(a)-(b). These bulges and oblique slip lines were produced by the shear failure plane of UHPC core and the restraint of the steel tube to restrict this shear failure plane. The shear failure in this study seems to be consistent with that of some previous studies on steel tube confined HSC or UHPC columns conducted by Xiong *et al.* (2017), De Oliveira *et al.* (2010), Johansson and Gylltoft (2001), and Schneider (2006).

3.2 Axial load versus axial strain curves

The measured axial load versus axial strain (L-S) curves of all specimens are illustrated in Fig. 6. The axial displacement of specimens in each loading interval was calculated by subtracting the summation of elastic displacements of two steel blocks from the average displacement recorded by three LVDTs. Subsequently, the axial strain of specimens was calculated from this axial displacement divided by the overall length of the concrete core (L_c).

It is evident from Fig. 6 that all specimens experienced an almost linear ascending part and a short elasto-plastic stage before the ultimate load, then followed by a decrease of load capacity until reaching a relatively stable residual strength (or a second peak load), at which a slight recovery stage of the strength or a or a virtually horizontal branch developed. Previous studies indicated that the shear failure is associated with a softening branch in L-S curves (Johansson 2002). The softening branch right after the ultimate load is marked by a drop of load from the ultimate load (N_u) to the second peak load (N_{res}), this is caused by the brittle nature of UHPC. Beyond this sudden drop of load, a larger expansion of the UHPC core leads to a contact with the outer steel tube. Therefore, in the post-peak stage, a significant confinement provided by the steel tube effectively prevents the shear failure of the concrete core, thereby improving the ductility. The larger confining stress and the hardening effect of steel tube in tension compensate the strength degradation of concrete, thus leading to a strength recovery.

Fig. 6 also shows the effect of column length on the L-S curves. As expected, the short columns (with L=600 mm) generally exhibited a more ductile behavior in the post-peak stage and a smaller magnitude of strength loss after the ultimate load as compared to the intermediate columns (with L=1000 mm). It is interesting to explore in Fig. 6 that beyond the ultimate load, the columns with the smallest steel thickness of 5.0 mm performed a horizontal branch, while the remaining columns with larger steel thickness of 6.3 mm and 8.8 mm showed a descending branch. This is likely explained by the fact that the steel tube with thickness of 5.0 mm had a highest tensile strength and its stress-strain curve showed a strain hardening stage right after the yield strength, while the steel tube with thickness of 6.3 mm and 8.8 mm showed a plateau branch. Moreover, the shape of stress versus strain curves of steel coupons with thickness of 5.0 mm was found to adapt with high strength steel, whereas the shape of two remaining steel coupons with thicknesses of 6.3 and 8.8 mm was preferable to mild steels. This exploration implies that high strength steel should be used for this type of columns in order to obtain more significant increase in the ductility of columns. This inference is in line with that of previous studies by (Xiong et al. 2017). However, due to a limited amount of tests in this study with considering various steel yield strength, this finding should be experimentally or numerically checked further.

The longitudinal and hoop strains in the steel tube were recorded at the mid-height by the uni-axial strain gauges placed at the outer surface of the steel tube. At the mid-height section, there were three strain gages measuring the hoop strains and three strain gages measuring the longitudinal strains. To investigate the stress state of steel tube at the mid-height section, these average values of strains were converted into average values of stress by

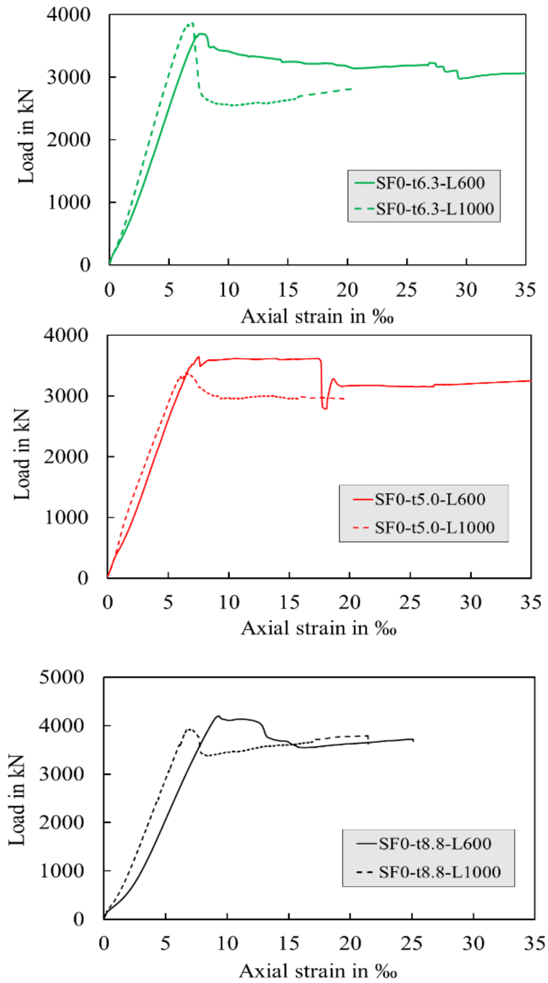

Fig. 6 L-S curves of test specimens

using the elastic-plastic analysis method proposed by Zhang et al. (2005). Fig. 7 shows the load versus stress curves of the steel tube at the mid-height. As depicted in Fig. 7, in the elastic stage of load versus axial strain response of the columns, the longitudinal and hoop stresses increased linearly at the initial loading stage. When the axial load was close to the ultimate load of unconfined concrete (f_c), the longitudinal and hoop stresses showed nonlinearity and increased rapidly. It could be observed that although noload was applied on the steel tube directly, the longitudinal stress at the mid-height section increased quickly due to the bonding resistance between the concrete core and the steel tube. the hoop stress maintained at an extremely low level up to the ultimate load. Although the hoop stress beyond the ultimate load were not performed herein, it is believed that the values of hoop stress at the mid-height of the steel tube would significantly increase and exceed the yield stress of steel in the post-peak stage of load versus axial strain response of the columns.

3.3 Effect of steel tube

Fig. 8 depicts the effect of steel thickness on the L-S curves. The applied loads (N) were normalized with respect to the nominal cross-sectional capacity of the concrete core ($A_c.f_c$). In order to investigate the effect of steel thickness on

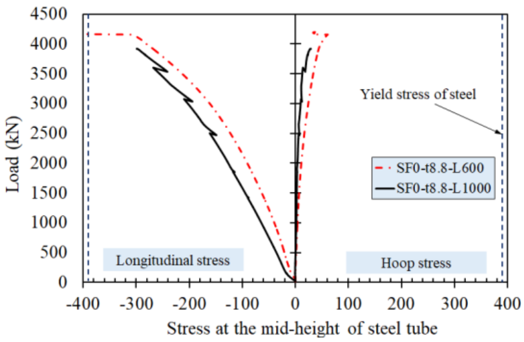

(a) Columns with thickness of 8.8 mm

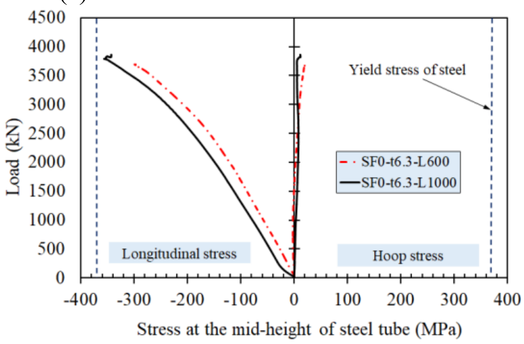

(b) Columns with thickness of 6.3 mm

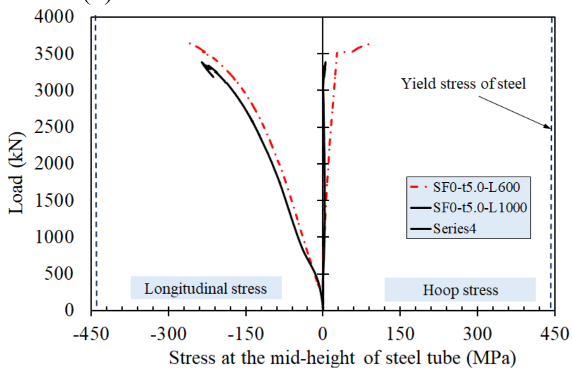

(c) Columns with thickness of 5.0 mm

Fig. 7 Load versus stress curves of the steel tube at the mid-height

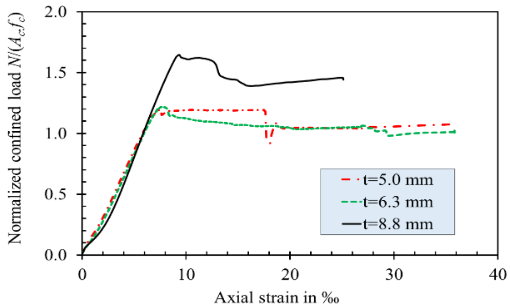

(a) Short columns

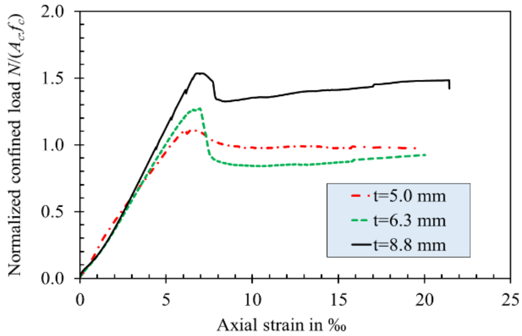

(b) Intermediate columns

Fig. 8 Effect of steel tube thickness on L-S curves

L-S curves, the normalized confined loads $N/(A_c.f_c)$ were plotted against the axial strains for each group of short and intermediate columns.

In general, there is no noticeable increase in the initial stiffness as steel thickness increases from 5.0 mm to 8.8 mm. As expected, the columns with a largest steel thickness of t = 8.8 mm (or a highest confinement index ξ) exhibited the most significant increase in the normalized peak strength. As compared to the unconfined concrete strength, the confined strengths of these columns were significantly increased by 65%, 22% and 20% in the case of the short columns with steel thicknesses of t = 8.8, 6.3 and 5.0, respectively, and also increased by 54%, 27% and 12% in the case of the intermediate columns with steel thicknesses of t = 8.8, 6.3 and 5.0, respectively. When steel thickness increased from 5.0 mm to 6.3 mm, there was almost no increase in the normalized peak strength. This may be due to that the confinement index ξ of the columns having steel thickness of t = 5.0 mm is quite close to that of the columns having steel thickness of t = 6.3 mm.

In addition to the beneficial effect of higher steel thickness (or higher confinement index ξ) on the strength enhancement and the elasto-plastic stage within the pre-peak stage of L-S curves, the use of larger steel thickness was found to decrease the slope of the descending branch. Besides, it is worth noting that all the columns with t = 8.8 mm presented a more pronounced strength recovery in the L-S curves. The recovery stage is attributed to the effect of strain hardening of steel tube and the stronger confinement effect induced by higher steel thickness. Despite of having an almost identical confinement index to the columns with t = 6.3 mm, the columns with t = 5.0 mm displayed a better post-peak behavior than that in the columns with t = 6.3 mm. This can be explained by the fact that the yield strength of the steel tube with t = 5.0 mm at the value 445.9 MPa is much higher than that of the steel tube with t = 6.3 mm at the value 373.4 MPa.

To quantify the effect of steel thickness on the strength and the ductility of columns, the values of strength enhancement ratio *SR* and ductility index *DI* were plotted against the ratios of *D/t* for three short and three intermediate columns. The strength enhancement ratio (*SR*) introduced by Han et al. (2005) provides a quantitative measure of the strength enhancement arising from the composite action in STCC columns:

$$SR = \frac{N_u}{A_c \cdot f_c} \tag{1}$$

where N_u is the ultimate load obtained from the experimental test, A_c is the cross-sectional area of the concrete core, and f_c is the concrete cylinder strength.

The ductility of the specimens is assessed by means of the ductility index *DI* (Han *et al.* 2005, An and Fehling 2017b)

Table 4 Test results of N_u, N_{res}, *DI* and *SR*

Specimens	ξ	N_u (kN)	N_{res} (kN)	*DI*	*SR*
SF0-t5.0-L600	0.34	3645.94	3193.85	2.34	1.20
SF0-t6.3-L600	0.36	3692.81	3165.12	2.56	1.22
SF0-t8.8-L600	0.61	4200.84	3570.71	1.88	1.65
SF0-t5.0-L1000	0.34	3383.35	2962.26	3.09	1.12
SF0-t6.3-L1000	0.36	3861.14	2570.15	1.05	1.27
SF0-t8.8-L1000	0.61	3919.86	3331.88	1.21	1.54

$$DI = \frac{\varepsilon_{85\%}}{\varepsilon_u} \quad (2)$$

in which $\varepsilon_{85\%}$ is the axial strain when the load decreased to 85% of the ultimate load, and ε_u is equal to the axial strain at the ultimate load.

The confinement index ξ was used to reflect the combined effect of f_c, f_y, *D/t*:

$$\xi = \frac{f_y \cdot A_s}{f_c \cdot A_c} \quad (3)$$

Three types of steel thicknesses t = 5.0 mm, 6.3 mm and 8.8 mm corresponds to *D/t* ratios of 30.48, 24.19 and 17.32, respectively. An increase in steel tube thickness also corresponds to a decrease in the ratio of *D/t* and an increase in the confinement index. Fig. 9 shows the effect of *D/t* ratios on *SR* and *DI*, while Table 4 presents the results of N_u, N_{res}, *DI* and *SR* for all columns. As reported in Table 4 and Fig. 9, for all columns, there was no noticeable increase in *SR* when the steel thickness increases from 5.0 mm to 6.3 mm, this can be attributed to the almost identical confinement indices of these two types of steel thickness. However, when increasing steel thickness from 5.0 mm to 8.8 mm, *SR* was increased by 45% for the short columns, while *SR* was increased by 42% for the intermediate columns. Therefore, the strength enhancement is increased with increasing the steel thickness. The ductility index *DI* is mainly dependent on the level of confinement effect. It can be seen that the influence of *D/t* ratio on *DI* was irregular; this accords with a large variation in the post-peak region of L-S curves as changing steel thickness. For instance, when steel thickness decreased from 8.8 mm to 5.0 mm, *DI* values tended to increase. The significant improvement in the ductility of the post-peak response of the columns with the use a smallest steel thickness (t = 5.0 mm) as observed above implies that in addition to the impact of the steel thickness, the post-peak softening rate is also affected by the increase in the yield strength of the steel tube. Within this study, no effort to comprehensively examine the effect of the yield strength of the steel tube was made due to the limited test specimens.

4. Load contribution of the steel tube and the concrete core to the total load

The longitudinal and hoop stress distribution along the height of circular STCC columns were numerically

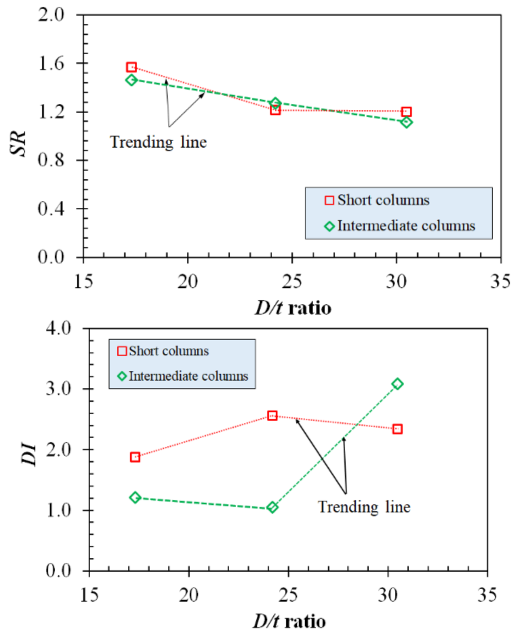

Fig. 9 Effect of *D/t* ratios on *SR* and *DI*

investigated by Yu *et al.* (2010), Haghinejad and Nematzadeh (2016), and Gupta *et al.* (2014). These authors pointed out that the distribution of the longitudinal and hoop stress is non-uniform, thus leading to the non-uniform distribution of the confinement stress throughout the length of the columns. Gupta *et al.* (2014) supposed that the confinement induced by the steel tube is almost uniform along the periphery of the steel tube. It was found in these studies that at the columns ends, the longitudinal stress of the steel tube is zero, whereas the hoop stress is relatively high. In contrast, the numerical results of Yu *et al.* (2010) revealed that, the longitudinal stress tends to increases and the hoop stress gradually decreases from the column ends toward the column mid-height. Similar to Yu *et al.* (2010), Haghinejad and Nematzadeh (2016) stated that at the column mid-height, the confining stress due to the development of the hoop strain is smallest, while the longitudinal stress is maximum. Observing the increasing rate of strains on the outer steel tube in the circular STCC columns, Han *et al.* (2008) reported that the increase of the hoop strain values at the top of the columns is quicker than that in the middle of the columns, but the increase of longitudinal strain values in the middle of the columns tends to be faster than that at the top of the columns. To investigate the stress state of the steel tube along the length of the columns, Schneider (2006) used the strain gauges attached to the steel tube at three levels (1, 2 and 3) to monitor the steel strains at three areas as shown in Fig. 10. From the experimental results, the author also reached a conclusion that the hoop stress of the steel tube is highest at the position near the column ends (level 1) and the longitudinal stress of the steel tube is highest at the column mid-height (level 2). Accordingly, the calculated confining stress at the level 1 were higher than those at the other levels. This can be due to the effects of the friction between the loading steel blocks and the concrete core at the columns ends, which can greatly exaggerate the additional confining stress and thus resulting in very high compressive

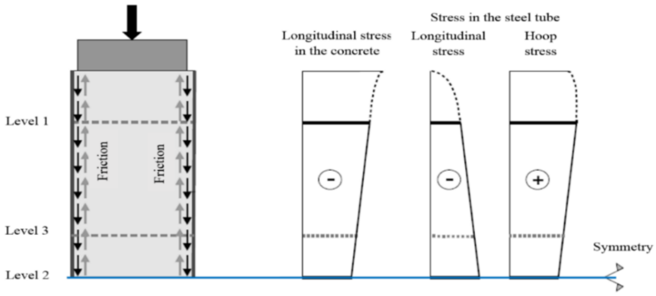

Fig. 10 Schematic of stress distribution in circular STCC columns (Reproduced from Schneider 2006)

stress for the concrete core in these areas (Gupta *et al.* 2014).

To investigate the stress state of steel tube at the mid-height section, the average values of strains recorded by strain gauges were converted into average values of stresses by using the elastic-plastic analysis method proposed by Zhang *et al.* (2005). From the discussion above, in each step of loading, the average value of longitudinal stress at the mid-height of the columns can represent the maximum stress of the steel tube along the length of the columns. On the other hand, the average hoop stress at the mid-height cannot be adopted to calculate the confining stress because its value may be smaller than the hoop stress values in the other positions as explained above.

As is also mentioned above, the ascending branch up to the ultimate load were mainly associated with the development of the longitudinal stress in the steel tube and the concrete core, whereas the effect from the hoop stress in the steel tube can be negligible owing to its extremely small portion as compared to the longitudinal stress. Therefore, the load carried by the steel tube before the ultimate load (N_s) can be computed by multiplying the longitudinal stress of the steel tube (σ_v) at the mid-height and the area of steel cross section (A_s):

$$N_s = \sigma_v A_s \tag{4}$$

Although the load applied on the concrete core only, the load is partially transferred from the concrete core to the steel tube due to the existence of the bonding resistance. Hence, the total load applied on the composite column (N) in each loading step before the ultimate load is calculated as:

$$N = N_s + N_c \tag{5}$$

in which, N_s and N_c is the loads carried by the steel tube and the concrete core, respectively, in the loading process.
The longitudinal stress in the concrete core σ_{cc} is derived from the load carried by the concrete core N_c:

$$\sigma_{cc} = \frac{N_c}{A_c} \tag{6}$$

To quantify the load contribution of the steel tube and the concrete core to the total load at each loading step, the portion of the total load N shared by the load carried in the steel tube N_s is depicted in Fig. 11. Accordingly, Fig. 11 shows the relation between the normalized axial load N/N_u

Table 5 The values of N_s and N_c

Specimens	N_s (kN) (at the ultimate load N_u)	N_s/N (in the ascending branch)	N_c (kN) (at the ultimate load N_u)	σ_{cc} (MPa)	σ_{cc}/fc
SF0-t8.8-L600	1557.82	*0.16*-**0.37**	2642.26	185.24	1.04
SF0-t8.8-L1000	1187.12	*0.25*-**0.30**	2505.69	175.66	0.98
SF0-t6.3-L600	859.13	*0.17*-**0.23**	2786.81	181.64	0.92
SF0-t6.3-L1000	991.00	*0.22*-**0.26**	2928.86	190.90	0.96
SF0-t5.0-L600	605.65	*0.08*-**0.17**	3255.49	204.52	1.07
SF0-t5.0-L1000	544.48	*0.11*-**0.16**	2838.87	178.34	0.94

and the steel load to the total load ratio N_s/N. Furthermore, the values of N_s and N_c at the ultimate load, and the ranges of the ratio N_s/N in the ascending branch of –S curves were also given in Table 5.

It is revealed from Fig. 11 that the steel tube generally maintained the same portion of the total load throughout the elastic stage of the load-axial strain response of the columns. For most of the columns, the load shared by the steel tube performed a slight increase in the elasto-plastic stage of L-S curves of the columns. Due to the natural roughness of the surface between the concrete core and the steel tube, the bonding resistance may be varied from the column to the column, thereby causing a variation of the steel load to the total load ratio N_s/N during the loading steep and at the ultimate load when compared among tested columns. The load contribution of steel tube is dependent on the bonding resistance between two materials. According to many previous studies (Johansson and Gylltoft 2002; Liu *et al.* 2016), the contribution of the steel tube to the total load increases with increasing the value of bonding resistance. This implies that the value of bonding resistance between the UHPC core and the steel tube should be further checked by the push-out tests.

Bold words refer N_s/N at the ultimate load N_u; Italic words denote the average value of N_s/N in the elastic stage Fig. 11 shows that the intermediate columns had the ratio N_s/N considerably higher than the short columns, this is due to the larger bonding resistance induced by the higher length of the contact surface between the concrete core and the steel tube in the intermediate columns. Comparing among three steel tube thicknesses of 8.8 mm, 6.3 mm and 5.0 mm, it is demonstrated from Fig. 11 and Table 5 that

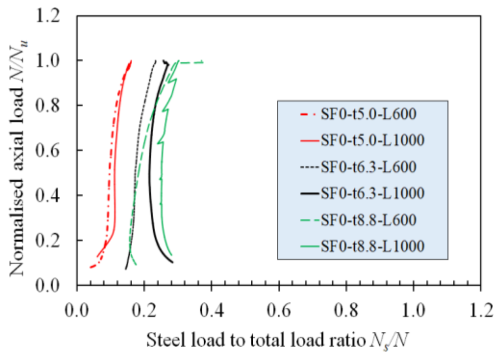

Fig. 11 The load contribution of the steel tube to the total load

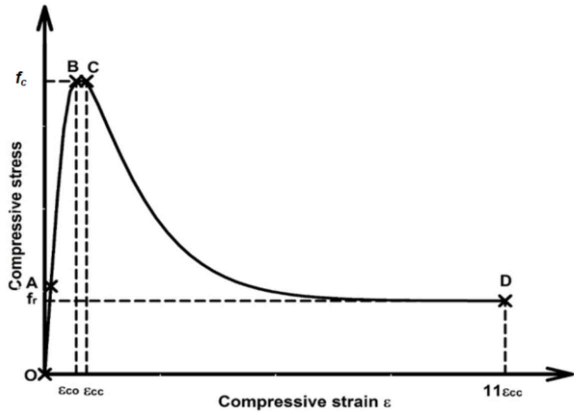

Fig. 12 Concrete stress-strain curve

there is an increasing tendency in the values of N_s/N with increasing the steel tube thickness. Therefore, the contribution of steel tube to the total load is higher with larger steel tube thickness. This inference is also true when using higher confinement index ξ.

As seen in Table 5, the confined stress in the UHPC core is quite close to the unconfined compressive strength with the ratio σ_{cc}/fc ranged between 0.92 and 1.04. This observation indicates that the increase in the compressive strength of UHPC core due to the confinement effect is minor. When reaching the unconfined compressive strength, UHPC core was crushed before steel tube yielded. Therefore, no significant confinement effect can be developed in the pre-peak stage of L-S curves. The confinement effect mainly affects to the behavior of columns in the post-peak stage of L-S curves. Also, the loading capacity of all STCC columns in this study is lower or slighly higher than the sum of the sectional capacity of the steel tube and UHPC core. This finding is in line with the studies conducted by Liew and Xiong (2012) and Xiong *et al.* (2017).

5. Comparison between FEM and test results

5.1 Finite element model details

5.5.1 Concrete core

By the steel tube surrounding the concrete core and providing peripheral stress, the concrete core undergoes tri-axial stresses and its compressive strength as well as its ductility enhances significantly. The concrete core being under a state of tri-axial stresses has different behavior throughout the loading. In order to correctly simulate the response of the concrete filled steel tubular columns, the tri-axial response of the concrete has to be modeled. One way to do it is by using the Damage Plasticity model available in the commercial code ABAQUS. This model can be utilized by inputting the following three parameters:

- The dilation angle of concrete ψ.
- The ratio of the second stress invariant on the tensile meridian to that on the compressive meridian K_c
- The ratio of the compressive strength under biaxial loading to uniaxial compressive strength (f_{bo}/f_c)
- The value of ψ can be calculated based on the work done by Tao et al. (2013):

$$\psi = \begin{cases} 56.3\cdot(1-\xi) \, for \xi \le 0.5 \\ 6.672\cdot e^{\frac{7.4}{4.64+\xi}} \, for \xi > 0.5 \end{cases} \tag{7}$$

where, ξ is the confinement factor and can be calculated as in Eq. (3)

The value of K_c can be found based on the equation developed by Tao et al. (2013) and Yu et al. (2010)

$$K_c = \frac{5.5}{5+2\cdot\left(f_c^{0.075}\right)} \tag{8}$$

The value of (f_{bo}/f_c) can be determined according to the equation proposed by Papanikolaou et al. (2007):

$$\frac{f_b}{f_c} = 1.5\cdot f_c^{-0.075} \tag{9}$$

The stress-strain curve proposed by Binici (2005) and modified by Al-Ani (2017) is adopted and illustrated in Fig. 12:

It has been assumed in this study that the concrete will reserve a linear behavior following the modulus of elasticity relationship from the beginning of the loading phase until the concrete reaches 30% of its compressive strength. Afterwards, the concrete stress from point A to point B follows the next equation which proposed by Binici (2005):

$$\sigma = f_e + (f_c - f_e)\cdot \frac{r\cdot\left(\frac{\varepsilon-\varepsilon_e}{\varepsilon_{co}-\varepsilon_e}\right)}{r-1+\left(\frac{\varepsilon-\varepsilon_e}{\varepsilon_{co}-\varepsilon_e}\right)} \tag{10}$$

where, f_e is the elastic concrete compressive strength, r is a constant, ε is the concrete strain and is bounded between ε_e and ε_{co}, ε_{co} is the unconfined compressive strain of concrete and ε_{cc} is the confined concrete compressive strain. ε_{co} can be calculated based on the work done in Al-Ani (2017) and Tasdemir (1998)

$$\varepsilon_{co} = \frac{30.02958\cdot f_c^{0.882933}+1160.756}{895673.2} \tag{11}$$

As suggested by Al-Ani (2017), it has been assumed that concrete will reserve the same stress from reaching the

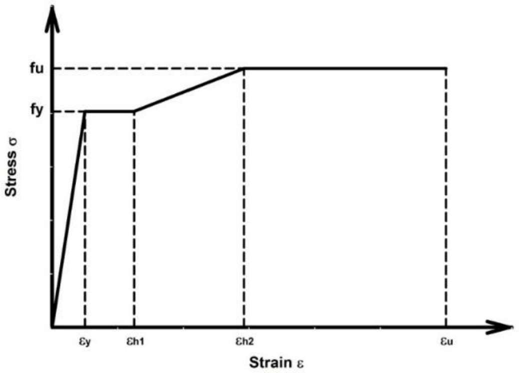

Fig. 13 Steel tube stress-strain curve

ultimate compressive strength at ε_{co} until it reaches its confined strain ε_{cc}, which can be determined by following the equation proposed in Attard and Setunge (2012) and modified in Al-Ani (2017):

$$\frac{\varepsilon_{cc}}{\varepsilon_c^{0.98377}} = 1.03549 + \left(13.88456 - 0.751 \cdot f_c\right) \cdot \left(\frac{F_B}{f_c}\right)^{080358} \quad (12)$$

where F_B is the confining stress provided to the concrete core by its surrounding steel tube, and can be calculated using the equation proposed by Tao et al. (2013):

$$F_B = \frac{\left(\left(1 + 0.027 \cdot f_y\right) \exp\left(-0.02 \cdot \frac{D}{t}\right)\right)}{1 = \left(1.6 \cdot \frac{f_c^{4.8}}{10^{10}}\right)} \quad (13)$$

The last part of the concrete's stress-strain curve can be calculated by following the equation proposed by Binici (2005):

$$\sigma = f_r + \left(f_c - f_r\right) \cdot EXP\left(-\left(\frac{\varepsilon - \varepsilon_{cc}}{\alpha}\right)^{\beta}\right) \quad (10)$$

5.1.2 Steel tube

The multilinear stress-strain curve of the steel material given in Fig. 13 which has been used in Al-Ani (2017) to simulate the response of the steel tube when surrounding concrete with strength ranged from 32 MPa to 102 MPa is adopted in this paper to simulate its response when infilled with concrete of strengths ranging from 178.9 MPa to 198 MPa.

Steel's modulus of elasticity E_s is assumed to be 200 GPa. ε_{h1} stands for the strain at the beginning of the hardening portion of the steel tube, and can be determined by the equation proposed in Al-Ani (2017):

$$\varepsilon_{h1} = \begin{cases} \frac{-7 \cdot f_y + 7100}{500} \cdot \varepsilon_y \left(f_y < 800MPa\right) \\ 3 \cdot \varepsilon_y \left(f_y \geq 800MPa\right) \end{cases} \quad (14)$$

ε_{h1} stands for the point that the steel tube reaches its ultimate yield strength, and can be determined also by the work done in Al-Ani (2017):

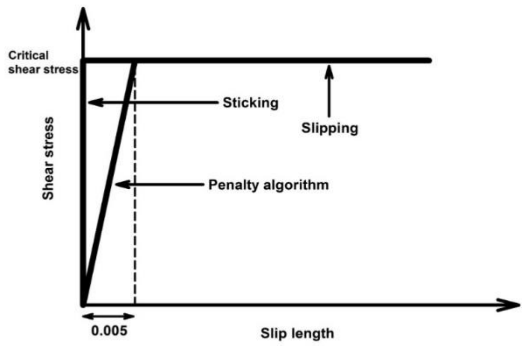

Fig. 14 The Coulomb friction model combined with the penalty algorithm

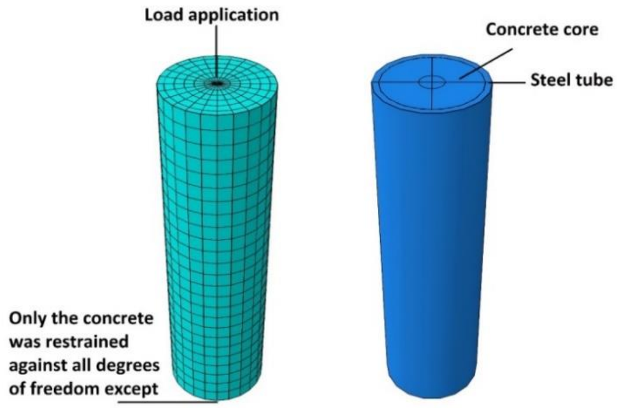

Fig. 15 Details of the FE model

$$\varepsilon_{h2} = \frac{f_u - f_y}{0.012 \cdot E_s} \quad (15)$$

The ultimate yield strength can be determined based on the equation suggested in Tao et al. (2013):

$$\text{when } 200 \leq f_y < 400: \quad f_u = 1.6 - 2 \cdot 10^{-3}\left(f_y - 200\right) \cdot f_y \quad (16)$$

$$\text{when } 400 \leq f_y < 800: \quad f_u = 1.2 - 3.75 \cdot 10^{-4}\left(f_y - 400\right) \cdot f_y \quad (17)$$

5.1.3 Interaction between the steel tube and the concrete core

A hard contact is employed to simulate the interaction behavior between concrete and steel along with the penalty algorithm method to control the contact clearance and contact pressure. Consequently, Coulomb friction model used to simulate the interaction in the tangential direction. A representation sketch of the Coulomb friction model combined with the penalty algorithm can be seen in Fig. 14 More details of the employed model can be found in Tao *et al.* (2013) and Al-Ani (2017).

5.1.4 Boundary conditions, load application, and mesh details

To make sure that the simulation duplicates the tests, the bottom end of the concrete core was fixed against all degrees of freedom. While, the upper end of the concrete

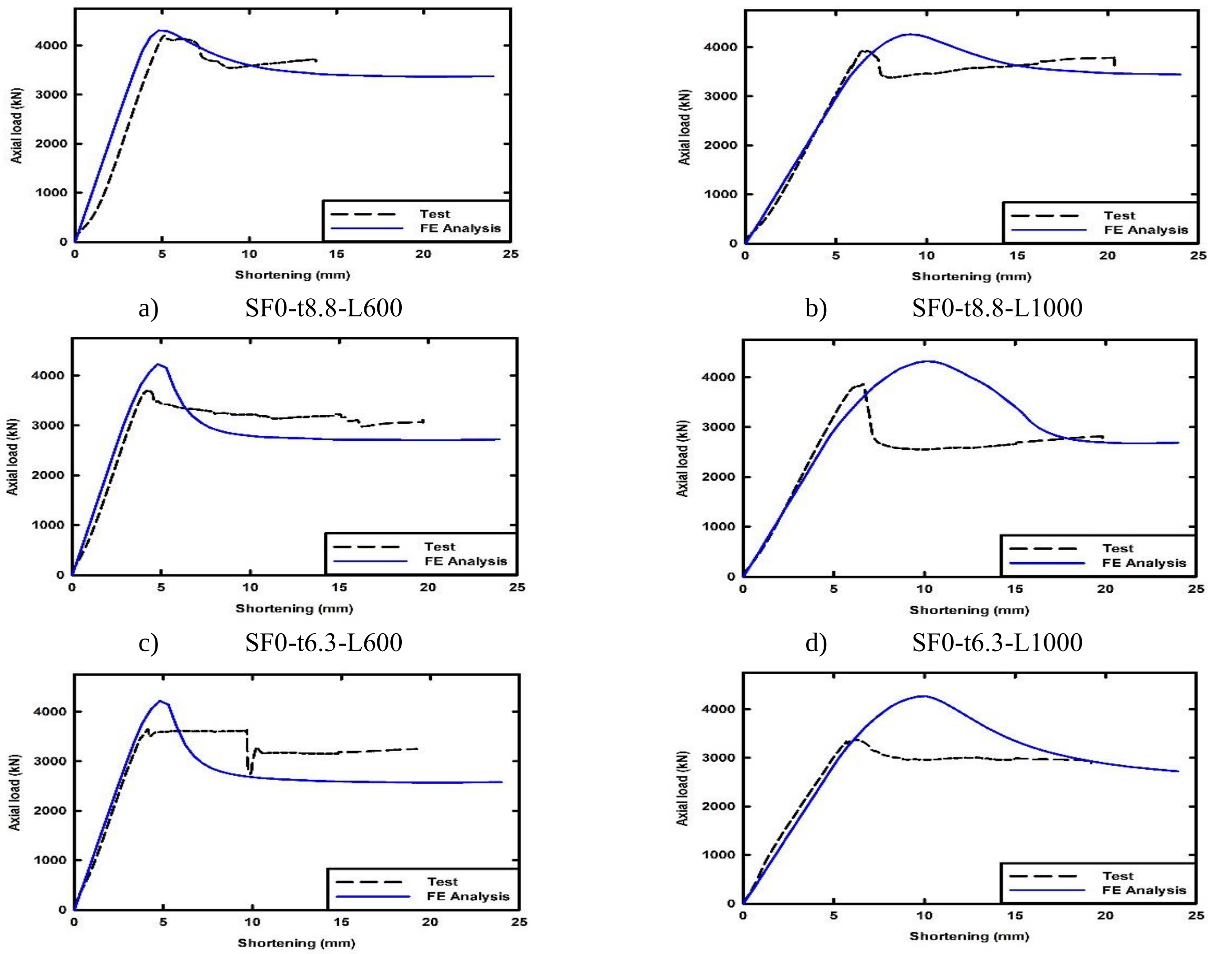

a) SF0-t8.8-L600 b) SF0-t8.8-L1000

c) SF0-t6.3-L600 d) SF0-t6.3-L1000

e) SF0-t5.0-L600 f) SF0-t5.0-L1000

Fig. 16 Load-shortening curves of the current FE model and experimental results for the selected specimens

core was fixed against all degrees of freedom except the one in the axial direction. The load was made by applying displacement on the upper end of the specimen. It should be noted here that only the concrete core was loaded in this study as this was the method followed in the tests. It is also worth to mention here that the same FEM has been used and verified before in Al-Ani (2017) for strengths ranged from 23 MPa to 102 MPa. This study investigates its performance when UHPC with strengths ranging from 178.9 MPa to 198.0 MPa are used. Fig. 15 depicts the simulated specimen.

5.2 Results and discussion

As mentioned before, the FEM was used to verify when the concrete compressive strength ranging from 23 MPa to 102 MPa (Al-Ani 2017). In this study, 6 specimens of UHPC without steel fibers with compressive strength ranging between 178.9 MPa to 198 MPa were analyzed in order to check the performance of the FEM against experimental results.

As can be seen from Fig. 16, there is, in general, a good agreement between the FEM and the test results of the short specimens with steel tube length equal to 600 mm in terms of ultimate load and post-peak behavior. On the other hand, it has been noticed that the current FEM overestimates the ultimate load and fails to accurately simulate the post-peak behavior of the intermediate specimens with steel tube length equal to 1000 mm. The failure noticed from the tests with sudden reduction in the columns load bearing after reaching its maximum. However, the simulation of the first intermediate column SF0-t8.8-L1000 showed acceptable performance in terms to both the ultimate load and the post-peak behavior. Main reasons behind this phenomenon might be explained as there is a higher influence from the parameter L_c/D and the length of the specimen when associated with UHPC. It is expected that the parameter (f_{bo}/f_c) adopted in this paper does not encounter the influence from the columns local buckling when UHPC is used in this type of columns. Therefore, it is suggested that more modification is required to address these limitations by investigating the influence of the column's length on the ratio (f_{bo}/f_c) .

In order to understand the interaction and the contact behavior between the two components, the concrete core and the steel tube, the contact-related results are illustrated in Fig. 17. This is done by comparing the confining pressure, shear stress, and the slip length of the different contacted elements located between the concrete and the steel elements. The confining pressures at different lengths

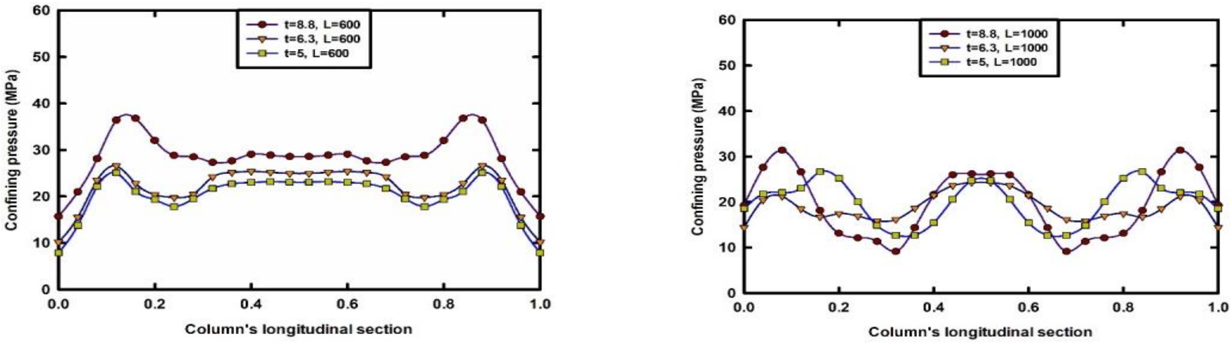

(a) Short columns (b) Intermediate columns

Fig. 17 The confining pressure along the simulated specimens.

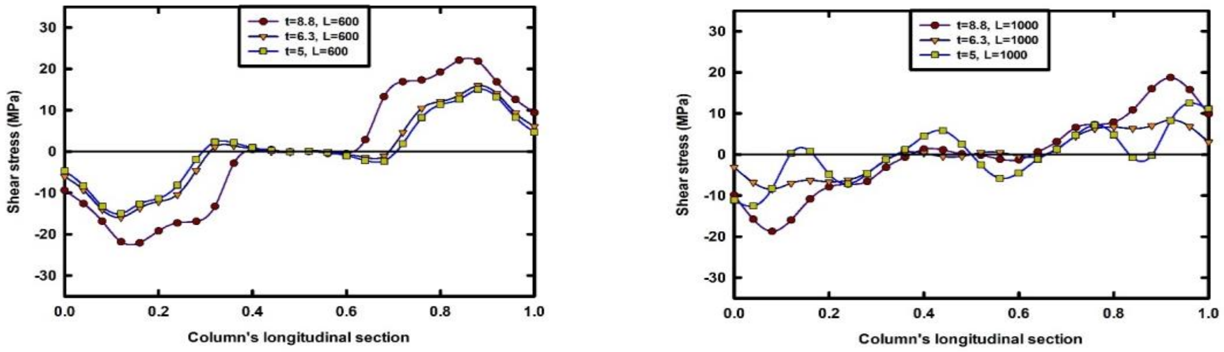

(a) Short columns (b) Intermediate columns

Fig. 18 The shear stress along the simulated specimens.

were collected at the ultimate load. As seen in Fig. 17, although the lateral deformation of the concrete core at the two ends of STCC columns is prevented and smaller than lateral deformations at different height. The confining pressures were observed to be larger than 10 MPa at the ultimate load. The effect of stress concentration due to end conditions causes a significant pressure on the concrete core. As compared to short CFST columns, Yu *et al.* (2010) stated that the confining stress of short STCC columns is generally higher. Fig. 17 depicts the recorded confining pressure along the longitudinal direction of the specimen. As can be seen from Fig. 17(a), with the short specimens with steel thickness t = 8.8 mm, the confining pressure recorded its highest value somewhere at 15 - 20% of the specimen's length from both ends. The center of the specimen recorded almost 9 MPa lower confining pressure than the highest values near the ends. This might be explained as this specimen has the highest steel content in its cross-section, 21.76%. Meanwhile, the other two short specimens having t = 6.3 mm and 5.0 mm with steel contents equal to 15.85% and 12.69%, respectively, recorded a confining pressure at the middle portion of the specimens almost as high as the recorded confining pressure near the two ends. Fig. 17(b) showed a different behavior. The confining pressure recorded lower value in the intermediate columns when comparing to the short columns. Moreover, it is noticeable that the pattern of the confining pressure curves is more steep in the intermediate columns. The locations of the maximum confining pressure were closer to the ends than the first group, about 10% from both ends. Also, all specimens recorded almost as high confining pressure at the middle portion as near the ends. Which means the influence of the steel content is reduced when increasing the length.

Fig. 18 demonstrates the shear stresses of the contacted steel and concrete elements along the simulated columns. Fig. 18(a) shows the shear stresses of the short specimens while Fig. 18(b) shows the shear stresses of the intermediate specimens. As can be seen, the maximum values of the shear stresses are located exactly at the same elements which recorded the maximum confining pressure near the ends. The middle portion, 40% - 60% of the specimen's length, recorded zero shear stresses and was the point where the direction of the shear stress changes to the opposite direction. It has observed that the shear stress's value increases when increasing the steel content. The specimens with t = 8.8 mm and 6.3 mm registered the highest value at exactly the same element which registered the highest confining pressure near the ends. The specimens with t = 5 mm recorded different pattern than the first two specimens but also indicated a connection to the confining pressure. Overall, the intermediate columns recorded lower shear stress value than the short columns.

Figs. 19(a)-(b) show the slip length of the steel tube and the concrete core contacted elements along the length of the short and the intermediate columns. It can be seen by examining the short columns that the maximum slip length happened at the end of the specimens. While the zero slip happened somewhere between 37% - 63 % of the column's length. Negative values of slip length mean movements in

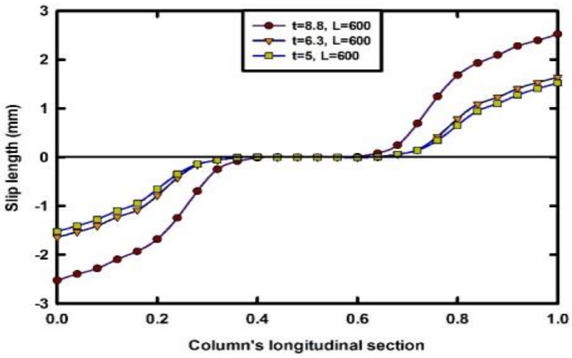

(a) Short columns

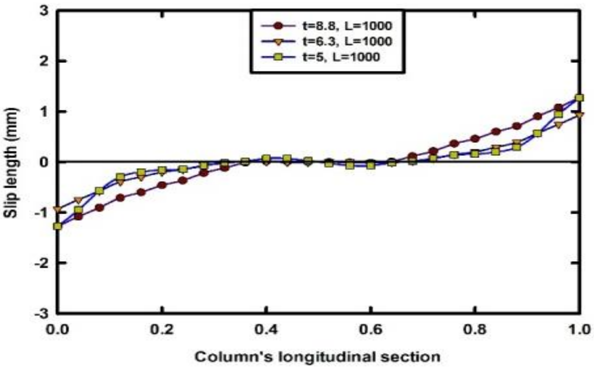

(b) Intermediate columns

Fig. 19 The slip length along the simulated specimens.

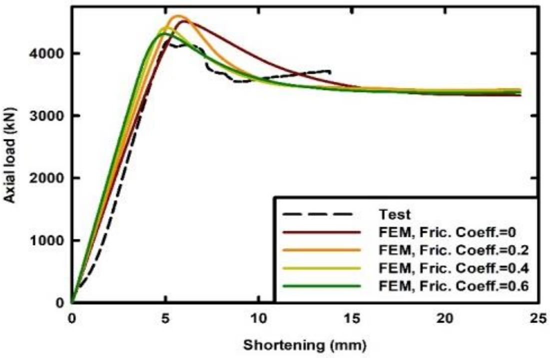

(a) Influence of friction coefficient on load-shortening curve

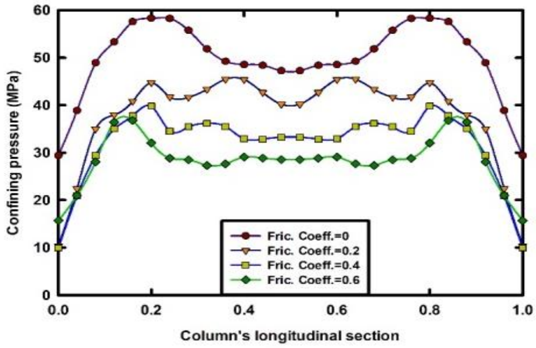

(b) Influence of friction coefficient on confining pressure

Fig. 20 Influence of friction coefficient on load-shortening curve and confining pressure

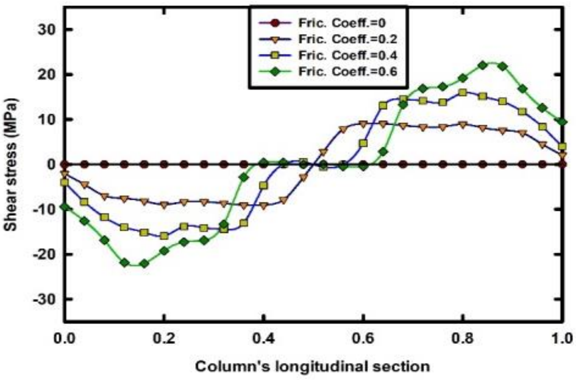

(a) Influence of friction coefficient on shear stress

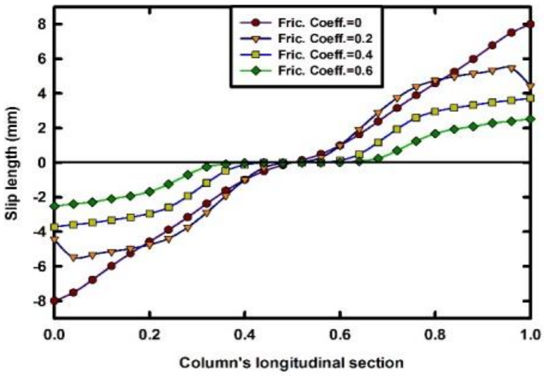

(b) Influence of friction coefficient on slip length.

Fig. 21 Influence of friction coefficient on shear stress and slip length

the opposite direction. There were not many different observations made in the intermediate columns. The only odd observation was that the intermediate columns resulted in a lower slip length value than that in the short columns.

More simulations have been run to investigate the influence of changing the coefficient of friction on the load-shortening curve, the confining pressure, the shear stress, and the slip length. The first specimen has been selected for this investigation with four different values of friction coefficient, 0, 0.2, 0.4, and 0.6, respectively. The reason behind choosing this specimen is basically because this specimen exhibited the most agreed simulation results to the experimental results. Fig. 20(a) illustrates a comparison between the load-shortening curve of the test results with the load-shortening curve calculated numerically by the FEM approach. As can be seen, decreasing the friction coefficient results in increase in the ultimate load and a more ductile performance added to the post-peak portion of the load-shortening curve. However, the specimen with zero friction coefficient exhibited a lower value of ultimate load, yet a more ductile post-peak of the load-shortening curve. Among all these curves, the curve with friction coefficient equal to 0.6 was the most agreed load-shortening curve to the experimental results when it comes to both the ultimate load and the post-peak behavior.

Fig. 20(b) shows that the confining pressure of simulated specimen. It shows that the friction coefficient has a significant role on the confining pressure. It indicates that the decrease in the friction coefficient increases the confining pressure significantly.

Figs. 21(a)-(b) illustrate the influence of changing the friction coefficient on the shear stress and the slip length,v respectively. It can be noticed from Fig. 21(a) that the value of the shear stress increases while increasing the friction coefficient from 0.2 to 0.6. When friction coefficient is zero, the shear stress also becomes zero along the height of the specimen. Fig. 21(b) shows the slip length along the height of the specimen. As can be seen, the value of the slip length increases when decreasing the friction coefficient. This is also consistent with the scientific sense, where in zero friction coefficient contacted specimens, a major movement can take a place. As in the comparison with the test data, the maximum slip length was recorded at the ends of the specimens.

6. Conclusions

This study is expected to enrich the existing test database of STCC columns and to supplement information about the confinement behavior of UHPC. On the basis of the experimental results, some conclusions can be drawn as follows:

- The compressive failure in all specimens occurred as a result of shear plane failure of the UHPC core, thus causing a softening branch in L-S curves beyond the ultimate load.
- Loading on only the UHPC core can lead to an enhancement in strength and ductility, and restrict the brittleness of unconfined UHPC.
- Within the tests in this study, confined strength reached 120%-165% and 112%-154% of unconfined strength for short and intermediate columns, respectively. Moreover, a prominent ductility with a large axial strain and a strength recovery in the post-peak stage was observed for all columns.
- An increase in steel tube thickness (or confinement index) results in an increase in the strength and ductility enhancement and a decrease in the slope of the descending branch of L-S curves. Besides, steel tube with higher yield strength can significantly improve the post-peak behavior.
- The contribution of steel tube to the total load is higher with larger steel tube thickness or higher confinement index.
- The confined strength of the columns is induced by the load contribution of the steel tube. The confinement effect significantly enhances the ductility of columns in the post-peak stage of L-S curves.
- The results of the simulation show a good agreement to the experimental results of the current FEM in both ultimate load and post-peak behavior of the short columns. However, limitations have encountered in both respects, ultimate load and post-peak behavior, when the intermediate columns are utilized. The main reason of this limitation can be attributed to the unexpected increased influence received from the length of the columns, in particular L_c/D, on the capacity of these columns.
- More research is required to deal with this shortcoming and it is suggested that the method of calculating the parameter f_{bo}/f_c should be revised to encounter this special type of concrete.
- The results of the simulation suggest that increasing the friction coefficient leads to a decrease in the ultimate load and the confining pressure.

References

Abbas, Y.R. (2017), “Nonlinear Finite Element Analysis to the Circular CFST Stub Columns”, *Procedia Eng.*, **173**, 1692–1699. https://doi.org/10.1016/j.proeng.2016.12.197.

Al-Ani, Y.R. (2016), “Finite element study to address the axial capacity of the circular concrete-filled steel tubular stub columns”, *Thin-Walled Struct.,* **126***,* 2–15. https://doi.org/10.1016/j.tws.2017.06.005.

An, L.H. and Fehling E.(2017*f*), “Numerical study of circular steel tube confined concrete (STCC) stub columns with various concrete strengths”, *J. Construct. Steel Res.*, **136**, 238-255. https://doi.org/10.1016/j.jcsr.2017.05.020.

An, L.H. and Fehling, E. (2017a), “A review and analysis of UHPC filled steel tube columns”, *Struct. Eng. Mech.*, **61**(2), 417-430. https://doi.org/10.12989/sem.2017.62.4.417.

An, L.H. and Fehling, E. (2017b), “Analysis of circular steel tube confined UHPC stub columns”, *Steel Compos. Struct.*, **23**(6), 669-682. https://doi.org/10.12989/scs.2017.23.6.669.

An, L.H. and Fehling, E. (2017c), “Assessment of axial stress-strain model for UHPC confined by circular steel tube stub columns”, *Struct. Eng. Mech.*, **63**(3), 371-384. https://doi.org/10.12989/sem.2017.63.3.371.

An, L.H. and Fehling, E. (2017d), “Influence of steel fiber content and type on the uniaxial tensile and compressive behavior of UHPC”, *Construct. Build. Mater.*, **153**, 790-806. https://doi.org/10.1016/j.conbuildmat.2017.07.130

An, L.H. and Fehling, E. (2017e), “Numerical analysis of steel tube confined UHPC stubs columns”, *Comput. Concrete*, **19**(3), 263-273. https://doi.org/10.12989/cac.2017.19.3.263.

Architectural Institute of Japan (AIJ) (2001), *Recommendation for Design and Construction of Concrete Filled Steel Tubular Structures*, AIJ, Japan.

Aslani, F., Uy, B., Tao, Z. and Mashiri, F. (2015), “Predicting the axial load capacity of high-strength concrete filled steel tubular columns”, *Steel Compos. Struct.,* **19**(4), 967-993. https://doi.org/10.12989/scs.2015.19.4.967.

Attard, M.M. and Setunge, S. (1996), “Stress-Strain Relationship of Confined and Unconfined Concrete”, *Mater. J.*, **93**, 432–442.

Binici, B. (2005), “An analytical model for stress–strain behavior of confined concrete”, *Eng. Struct.,* **27**, 1040–1051. https://doi.org/10.1016/j.engstruct.2005.03.002.

De Oliveira, W.L.A., De Nardin, S., De Cresce El Debs, A.L.H. and El Debs, M.K. (2010), “Evaluation of passive confinement in CFT columns”, *J. Construct. Steel Res.*, **66**(4), 487-495. https://doi.org/10.1016/j.jcsr.2009.11.004.

DIN 1048-5:1991-06, Prüfverfahren für Beton, Teil 5: Festbeton, gesondert hergestellte Probekörper, Normenausschuss für Bauwesen (NABau) im DIN Deutsches Institut für Norming e.V., Beuth Verlag GmBH, Berlin, Germany.

DIN EN 12350-8:2010-12, Testing fresh concrete - Part 8: self-compacting concrete-slump-flow test, German version EN 12350-8, 2010, Beuth Verlag, Berlin.

DIN EN 12390-3:2009-7, Testing hardened concrete-Part 3: Compressive strength of test specimens, German version EN 12390-3:2009, Beuth Verlag, Berlin.

Ding, F.X., Tan, L., Liu, X.M. and Wang, L. (2017), “Behavior of circular thin-walled steel tube confined concrete stub columns”, *Steel Compos. Struct.,* **23**(2), 229-238.

https://doi.org/10.12989/scs.2017.23.2.229.

Empelmann, M., Teutsch, M. and Steven, G. (2004), "Improvement of the post fracture behaviour of UHPC by fibres", *Proceeding of 2nd International Symposium on Ultra High Performance Concrete*, Kassel, March.

Empelmann, M., Teutsch, M. and Steven, G. (2008), "Load-bearing behaviour of centrically loaded UHPFRC-columns", *Proceeding of Second International Symposium on Ultra High Performance Concrete*, Kassel, March.

European standard EN 10002-1 (2001), Metallic material – Tensile testing – Part 1: Method of test at ambient temperature, Brussels, Belgium.

Graybeal B.A. (2005), "Characterization of the behavior of ultra-high performance concrete", Ph.D. Dissertation, University of Maryland, USA.

Gupta, P.K. and Singh, H. (2014), "Numerical study of confinement in short concrete filled steel tube columns", *Latin American J. Solids Struct.*, **11**, 1445-1462. http://dx.doi.org/10.1590/S1679-78252014000800010.

Giakoumelis, G. and Lam, D. (2004), "Axial capacity of circular concrete-filled tube columns", *J. Construct. Steel Res.*, **60**(7), 1049-1068. https://doi.org/10.1016/j.jcsr.2003.10.001.

Haghinejad, A. and Nematzadeh M. (2016), "Three-dimensional finite element analysis of compressive behavior of circular steel tube-confined concrete stub columns by new confinement relationships", *Latin American J. Solids Struct.*, **13**, 916-944. http://dx.doi.org/10.1590/1679-78252631.

Han L., Yao, G.H., Chen, Z.P. and Yu, Q. (2005), "Experimental behavior of steel tube confined concrete (STCC) columns", *Steel Compos. Struct.*, **5**(6), 459-84. https://doi.org/10.12989/scs.2005.5.6.459

Han, L.H.; Liu, W. and Yang, Y.F. (2008), "Behavior of thin walled steel tube confined concrete stub columns subjected to axial local compression", *Thin-Walled Struct.*, **46**, 155-164. https://doi.org/10.1016/j.tws.2007.08.029.

Johansson, M. (2002), "Composite action and confinement effects in tubular steel-concrete columns", Ph.D. Dissertation, Department of Structural Engineering, Concrete Structures, Chalmers University of Technology, Göteborg, Sweden.

Johansson, M. and Gylltoft, K. (2002), "Mechanical behavior of circular steel-concrete composite stub columns", *J. Struct. Eng.*, **128**(8), 1073-1081. https://doi.org/10.1061/(ASCE)0733-9445(2002)128:8(1073).

Liew, J.Y.R. and Xiong, D.X. (2012), "Ultra-high strength concrete filled composite columns for multi-storey building construction", *Adv. Struct. Eng.*, **15**(9), 1487-1503. https://doi.org/10.1260/1369-4332.15.9.1487.

Liu, J., Zhang, S., Zhang, X. and Guo, L. (2009), "Behavior and strength of circular tube confined reinforced-concrete (CTRC) columns", *J. Construct. Steel Res.*, **65**, 1447-1458. https://doi.org/10.1016/j.jcsr.2009.03.014.

Liu, J., Zhou, X. and Gan, D. (2016), "Effect of friction on axially loaded stub circular tubed columns", *Adv. Struct. Eng.*, **19**(3), 546-559. https://doi.org/10.1177/1369433216630125.

Papanikolaou, V.K. and Kappos, A.J. (2007), "Confinement-sensitive plasticity constitutive model for concrete in triaxial compression" *Int. J. Solids Struct,* **44**, 7021–7048. https://doi.org/10.1016/j.ijsolstr.2007.03.022.

Shin, H.O., Soon, Y.S., Cook, W.D. and Michell, D. (2015), "Effect of confinement on the axial load response of ultrahigh-strength concrete columns", *J. Struct. Eng.,* **141**(6): 04014151-1:04014151-12.
https://doi.org/10.1061/(ASCE)ST.1943541X.0001106.

Tao, Z., Wang, Z.B. and Yu, Q. (2013), "Finite element modelling of concrete-filled steel stub columns under axial compression". *J. Constr. Steel Res*. **89**, 121–131. https://doi.org/10.1016/j.jcsr.2013.07.001.

Tasdemir, M.A., Tasdemir, C., Akyüz, S., Jefferson, A.D., Lydon, F.D. and Barr, B.I.G. (1998), "Evaluation of strains at peak stresses in concrete: A three-phase composite model approach", *Cem. Concr. Compos.* **20**, 301–318. https://doi.org/10.1016/S0958-9465(98)00012-2.

Tue, N.V., Küchler, M., Schenck, G. and Jürgen, R. (2004b), "Application of UHPC filled tubes in buildings and bridges" *Proceeding of International Symposium on Ultra High Performance Concrete*, Kassel, Germany, March.

Tue, N.V., Schneider, H., Simsch, G. and Schmidt, D. (2004a), "Bearing capacity of stub columns made of NSC, HSC and UHPC confined by a steel tube", *Proceeding of First International Symposium on Ultra High Performance Concrete*, Kassel, Germany, March.

Xiong, M.X., Xiong, D.X. and Liew, J.Y.R. (2017), "Axial performance of short concrete filled steel tubes with high-and ultra-high-strength materials", *Eng. Struct.*, **136**, 494-510. https://doi.org/10.1016/j.engstruct.2017.01.037.

Yan, P.Y. and Feng, J.W. (2008), "Mechanical behavior of UHPC and UHPC filled steel tubular stub columns", *Proceeding of Second International Symposium on Ultra High Performance Concrete*, Kassel, Germany, March.

Yang, X., Zohrevand, P. and Mirmiran, A. (2015), "Behavior of ultrahigh-performance concrete confined by steel", *J. Mater. Civil Eng. ASCE*, **28**(10), 04016113-1: 04016113-8. https://doi.org/10.1061/(ASCE)MT.19435533.0001623

Yu, Q., Tao, Z., Liu, W. and Chen, Z.B. (2010), "Analysis and calculations of steel tube confined concrete (STCC) stub columns", *J. Construct. Steel Res.*, **66**(1), 53-64. https://doi.org/10.1016/j.jcsr.2009.08.003.

Yu, T., Teng, J.G., Wong, Y.L. and Dong, S.L. (2010), "Finite element modeling of confined concrete-I: Drucker-Prager type plasticity model", *Eng. Struct*., **32**, 665–679. https://doi.org/10.1016/j.engstruct.2009.11.014

Zhang, S., Guo, L., Ye, Z. and Wang, Y. (2005), "Behavior of steel tube and confined high strength concrete for concrete-filled RHS tubes", *Adv. Struct. Eng*., **8**(2), 101-116. https://doi.org/10.1260/1369433054037976.

Zohrevand, P. and Mirmiran, A. (2011), "Behavior of ultrahigh-performance concrete confined by fiber reinforced polymers", *J. Mater. Civil Eng. ASCE*, **23**(12), 1727-1734. https://doi.org/10.1061/(ASCE)MT.19435533.0000324

CC